Flexible traffic control of the synfire-mode transmission by inhibitory modulation: Nonlinear noise reduction

Takashi Shinozaki,[1,*] Masato Okada,[2,1] Alex D. Reyes,[3] and Hideyuki Câteau[1,4]
[1]*RIKEN Brain Science Institute, 2-1 Hirosawa, Wako, Saitama 351-0198, Japan*
[2]*Graduate School of Frontier Sciences, University of Tokyo, 5-1-5 Kashiwanoha, Kashiwa, Chiba 277-8561, Japan*
[3]*Center for Neural Science, New York University, 4 Washington Place, New York, New York 10003, USA*
[4]*Graduate School of Life Science and Systems Engineering, Kyushu Institute of Technology, 2-4 Hibikino, Kitakyushu, Fukuoka 808-0196, Japan*

(Received 18 May 2009; revised manuscript received 2 December 2009; published 22 January 2010)

Intermingled neural connections apparent in the brain make us wonder what controls the traffic of propagating activity in the brain to secure signal transmission without harmful crosstalk. Here, we reveal that inhibitory input but not excitatory input works as a particularly useful traffic controller because it controls the degree of synchrony of population firing of neurons as well as controlling the size of the population firing bidirectionally. Our dynamical system analysis reveals that the synchrony enhancement depends crucially on the nonlinear membrane potential dynamics and a hidden slow dynamical variable. Our electrophysiological study with rodent slice preparations show that the phenomenon happens in real neurons. Furthermore, our analysis with the Fokker-Planck equations demonstrates the phenomenon in a semianalytical manner.

DOI: 10.1103/PhysRevE.81.011913 PACS number(s): 87.19.lm, 05.10.Gg, 87.18.Sn, 87.80.Jg

I. INTRODUCTION

Inhibitory input to network of neurons or more generally excitable media can modulate their activity in a way more complex than the simple activity suppression. For instance, inhibitory input delivered to a physiologically modeled neuron but not the leaky integrate-and-fire (LIF) neuron, can paradoxically increase the firing probability if it is delivered at a right timing [1–3]. For a population of neurons, this increase in firing probability of a single neuron is interpreted as an increase in the number of firing neurons in a population due to inhibitory input [4]. Here, we demonstrate a mechanism by which inhibitory input also enhance the synchrony of population firing. We carefully study this synchrony enhancement, that was actually visible in our previous study [4] but out of focus there. We indicate that a nonlinear mechanism is responsible for this synchrony enhancement. The synchrony enhancement by inhibitory input shows a clear contrast to the previously studied synchronization of neurons in mutually connected neural networks [5], which was observed even for a linear neuron model.

For the best illustration of the synchrony enhancement in the feedforward setting, we take the so-called the synfire chain as an example [4,6–24] which is stable propagation of population firing of neurons. Let us consider the population firing that is described with a bell-shaped pulse packet [Fig. 1(a)] which indicates the number of firing neurons versus time [9]. The pulse packet is specified with the number of total firing, a, the degree of synchrony measured with the width, σ, and the peak time of the population firing, t. The present study shows that properly timed inhibitory input can enhance synchrony of a pulse packet ($\sigma\downarrow$). This generalizes the previous observations [1–4] that are interpreted as an increase in the number of firing neurons ($a\uparrow$) in the present context.

Our numerical simulations coupled with a dynamical system analysis reveal a mechanism through which the membrane potential histogram in a neural population gets sharpened by inhibitory input via a nonlinear effect. We refer to this effect as nonlinear noise reduction. Importantly, this nonlinear noise reduction occurs with a population of physiologically plausible neuron models but not the LIF model.

Furthermore, our electrophysiological experiments with rodent brain slice preparations demonstrate that this mechanism works also in real neurons. Finally, we demonstrate semianalytically with Fokker-Planck (FP) equations how the mechanism works. Thus, the present study points out the

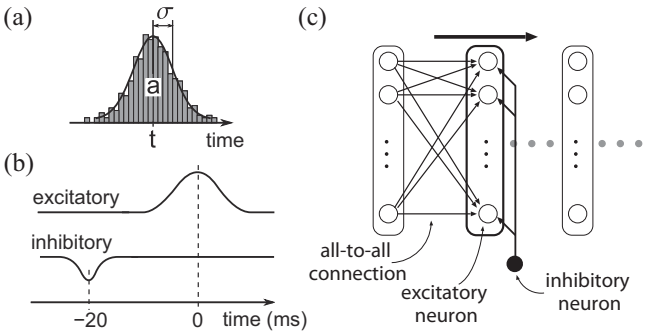

FIG. 1. Definition of a pulse packet and simulation setup. (a) Firing time histogram is parametrized with its total area, a, width, σ and peak time, t (a pulse packet) [9]. (b) Schematic illustration of the time course of excitatory (top) and inhibitory (bottom) synaptic currents. (c) Feedforward network of excitatory neurons which are modeled with Eqs. (1) and (2). Each neuron in a layer sends input to all the neurons in the following layer as in [9]. The excitatory neurons in the layer in the question (center) receive phasic inhibitory input with uniform strength at a specified timing. Open and filled circles, respectively, represent excitatory and inhibitory neurons.

*Present address: Center for Neural Science, New York University, 4 Washington Place, New York, New York 10003, USA.

importance of using physiological plausible neuron model to investigate the synchrony phenomenon in neuronal circuits.

II. NUMERICAL SIMULATIONS WITH A PHYSIOLOGICALLY PLAUSIBLE MODEL

Previous studies on the effects of inhibitory modulation [2–4] indicated that a hidden dynamical variable plays a pivotal role. Therefore, here we use a model proposed by Izhikevich [25] defined below, which is a minimal extension of the LIF model with an additional variable accounting for adaptation,

$$dv/dt = 0.04v^2 + 5v + 140 - u + I_{syn} + I_{bg}, \tag{1}$$

$$du/dt = a(bv - u), \tag{2}$$

where variables, v and u, represent membrane potential and adaptation. Currents, I_{syn} and I_{bg}, respectively, represent synaptic current and background current input. The background current, I_{bg}, is stochastic, and its actual value varies across neurons in a layer. In order to mimic the balanced excitation/inhibition, membrane potential shot noise [26] is employed for the background current input. It is modeled as sum of constant current and Gaussian white noise: $I_{bg}=\mu_{bg}+\sigma_{bg}W(t)$ with $\mu_{bg}=0.37$ mV, $\sigma_{bg}=1.70$ mV, $\langle W(t)\rangle=0$, and $\langle W(t)W(t')\rangle=\delta(t-t')$, which causes spontaneous firing of neurons in a layer at a rate consistent with *in vivo* observations (2–5 Hz). Variables v and u are reset as $v\rightarrow c$, $u\rightarrow u+d$ every time v crosses the threshold at 30 mV. As we explain later, the nonlinear noise reduction is supposed to be seen in a wide class of neuron models which involve nonlinear dynamics and at least one slow variable. The dynamics of Izhikevich model neuron satisfies both conditions. In our simulations, we set $a=0.02$, $b=0.2$, $c=-65$ and $d=8$, with which the model exhibits the typical regular spiking activity observed in real pyramidal neurons [25]. Variable u changes slowly because of its large time constant, $\tau_u=1/a=50$ ms.

Let us consider a feedforward network of excitatory neurons with all-to-all uniform interlayer connections [Fig. 1(c)]. To all the neurons in the layer in question, we assume that phasic inhibitory input is sent at a specified time. We then ask how a pulse packet propagation is affected by the modulating inhibitory input arriving 20 ms before the pulse packet arrival. Synaptic currents are modeled by alpha function, $f(t)=t/\tau^2\exp(-t/\tau)$, where τ is the time to the peak. We set $\tau=1.7$ ms for both excitatory and inhibitory synapses.

In order to examine how a shape of a pulse packet [a and σ in Fig. 1(a)] changes, we suppose that neurons in the initial layer [the leftmost one in Fig. 1(c)] fired in a manner whose population firing is described with a Gaussian-shaped pulse packet with $\sigma=5.0$ ms and $a=0.8N$ with N being the total number of neurons in a layer, and calculated the shape of a pulse packet generated at the next layer [the central one in Fig. 1(c)]. The initially prepared pulse packet and the generated pulse packet are respectively called an input packet and an output packet throughout the paper because they are input to and output from the central layer in Fig. 1(c). The arrival time of input packet is defined by the peak time, t [Fig. 1(b)].

Our inhibitory modulating input is adjusted to cause 5 mV of hyperpolarization [Fig. 2(c)]. This level of hyperpolarization is within the observed range of inhibitory postsynaptic potential (IPSP) elicited by a few neurons [27].

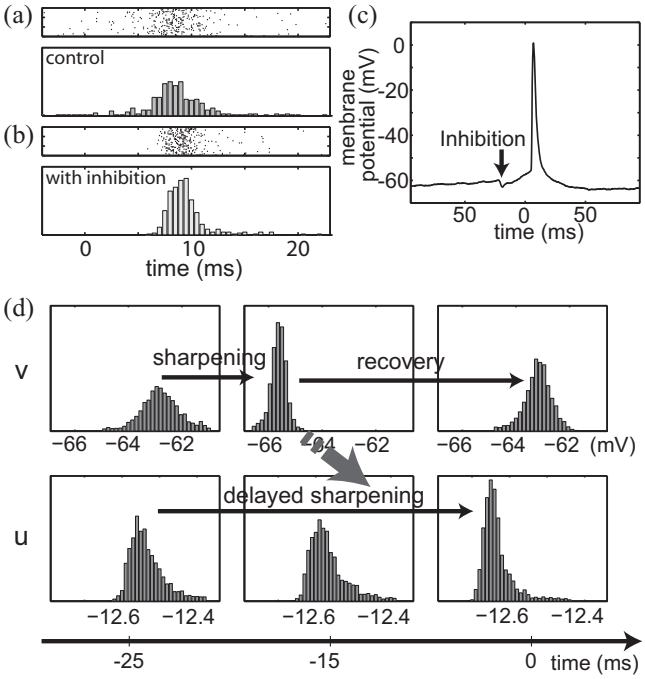

FIG. 2. Pulse packet sharpening demonstrated by numerical simulations in a single layer network. (a) and (b) Raster diagrams and the corresponding histograms showing neural spikes in response to an input packet of $a=0.8N$ and $\sigma=5.0$ ms, without (a) or with (b) preceding inhibitory input ($N=400$). (c) A sample voltage trajectory of a neuron in a layer. The small sag at $t=-20$ ms is caused by inhibitory input. (d) Histograms of v (top) and u (bottom) calculated and plotted at the initial moment ($t=-25$ ms), immediately after the inhibitory input is given ($t=-15$ ms) and at the arrival of the input packet ($t=0$ ms).

A feedforward network consisting of four hundred excitatory neurons per layer ($N=400$) [Fig. 1(c)] is simulated with a custom C code with 0.1 ms time steps. In order to obtain a pulse packet generated at the layer in response to an input packet, we use the same method as in [9]: we calculate firing time of each neuron in a layer by solving Eqs. (1) and (2) for each neuron in a layer. Because of the uncorrelated stochastic background input to each neuron, firing times vary within a layer. The resultant spike times are compiled in a histogram to shape an output packet.

Figures 2(a) and 2(b) clearly show that an output packet is sharpened by the phasic preceding inhibition. This enhanced synchrony of the population of neurons is particularly impressive if we note the small size of the IPSP [Fig. 2(c)]. Figure 2(d) shows the histograms of the values of the fast and slow variables at the initial moment (left), immediately after the arrival of the inhibitory input (middle) and at the arrival of the input packet (right). From Fig. 2(d), we notice that for the v histogram both the central value and its width mostly recovered their initial values at the arrival time of the input packet (right), while for the u histogram both values remain different from the initial values because of its slow dynamics.

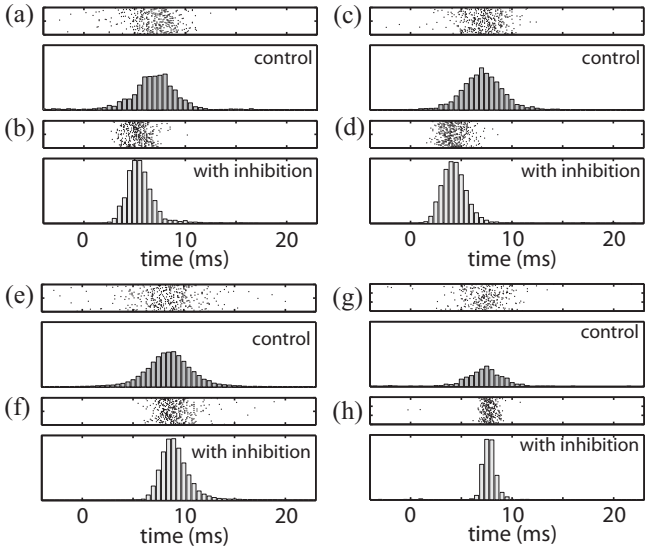

FIG. 3. Pulse packet sharpening demonstrated in various models in a single layer network. Shapes of output packets are calculated and depicted as Figs. 2(a) and 2(b). Output packets without (a), (c), (e), and (g) and with (b), (d), (f), and (h) the preceding inhibitory input. The noise reduction effect of the inhibitory input is obvious, suggesting the universality of the mechanism. (a) and (b)Izhikevich model mimicking the fast spiking neurons (a=0.1, b=0.2, c=−65, and d=2). (c) and (d) Izhikevich model mimicking the resonator neurons (a=0.1, b=0.26, c=−60, and d=−1). (e) and (f) Izhikevich model mimicking the regular spiking neurons but the number of neurons in a layer is large, N=40000. (g) and (h) Hodgkin-Huxley model neurons.

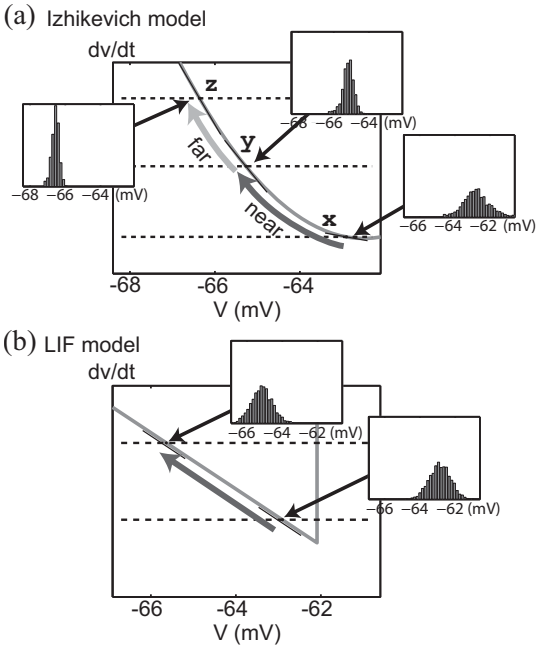

FIG. 4. Schematic illustrations of membrane potential dynamics. Each inset depicts the distribution of membrane potential at each point. A tangential slope at a point is proportional to the speed at which the scattered values of the membrane potential get back to the equilibrium point, thereby determines the width of the membrane potential distribution. (a) Dynamics of Izhikevich model. The parabola represents the curve of dv/dt versus v calculated with Eq. (1). Points x, y, and z represent three different levels of hyperpolarization (for details, see the text). If the membrane potential is initially near threshold, the fixed point moves from x to y. If it is initially far from threshold, the fixed point moves, for example, from y to z. (b) Dynamics of LIF model. The slope of the linear model as well as the corresponding width of the membrane potential distribution is constant everywhere and no noise reduction happens.

In Eq. (1), the reduced value of u increases the dc component on the right-hand side, which increases the firing probability ($a\uparrow$). This corresponds to the rebound firing described previously [1,2,4]. Meanwhile, the decreased width of the u histogram reduces the noise on the right hand of Eq. (1), thereby enhancing the synchrony of the output packet ($\sigma\downarrow$).

In order to confirm the generality of the nonlinear noise reduction effects among different conditions, we also perform numerical simulations with different parameter values of the Izhikevich model, with a larger network size, and with the Hodgkin-Huxley model. Figure 3 demonstrates the noise reduction effect by inhibitory input in all of the conditions, suggesting the universality of the nonlinear noise reduction.

III. MECHANISM

Here we explain how the nonlinear noise reduction of the dynamical variables crucially depends on the nonlinear dynamics. Since dv/dt depends quadratically on v [Eq. (1)], the curve for dv/dt versus v is represented as a parabola [see Fig. 4(a)]. Let us assume that input current, $I_{syn}+I_{bg}$, is not stochastic and takes a constant value. Depending on the constant value, the parabola shifts in vertical direction [see Eq. (1)]. Such shifts are equivalently illustrated by a moving horizontal axis (dotted lines) in vertical direction instead of moving parabola as in Fig. 4(a). Three points, x, y and z, indicate the zero crossing of the parabola (meaning dv/dt =0) for the constants of background current, μ_{bg}, being equal to 0.37, 0.30, or 0.23, and three dotted lines are corresponding equilibrium levels respectively. The background currents are not actually constant but have stochastic components which mimic the noisy conditions in the brain, therefore the membrane potential values are supposed to be distributed as illustrated in the insets of Fig. 4(a) for the three different conditions. When the membrane potential is kicked out of the equilibrium value by the noisy background input, the membrane potential tends to be attracted back to the equilibrium with the speed quadratically depending on v. Graphically, the speed is proportional to the vertical distance from the equilibrium which is represented by the dotted line in Fig. 4(a), which is large (small) when the tangential slope at that point is high (low). This is why the degrees of the scatter of the membrane potential are different among x, y, and z depending on their tangential slopes.

Suppose now that membrane potential values are distributed around x in Fig. 4(a). Inhibitory input to the neural population pushes the membrane potential distribution leftward and they get centered at y. Accordingly, the membrane

potential distribution is sharpened as shown in the corresponding inset [Fig. 4(a) at y]. On the other hand, if the membrane potential moves from around y to z, the membrane potential distribution is not expected to be sharpened largely. This explains that the bottom of the parabola [such as x in Fig. 4(a)] is the optimal starting position in reducing the variance of the membrane potential, thereby reducing the width of the pulse packet.

Two conditions are crucial for the effective noise reduction explained here. First, neurons should be moderately depolarized by the background input to exhibit spontaneous firing at a low rate as at x. If the neurons are hyperpolarized and totally silent, the initial membrane potential histogram is already narrow as at y and no more noise reduction is expected [see Fig. 4(a) at z]. Second, the membrane potential dynamics needs to be nonlinear. For the linear model [Fig. 4(b)], the tangential slope is constant everywhere and no noise reduction occurs.

Note however that this nonlinear noise reduction manifests a visible effect only if the dynamics includes a slow hidden variable. Since the inhibitory input implies not only the reduction in the width of the membrane potential histogram but also the significant reduction in the mean value of it [Fig. 2(d)], middle panel in the top row). With this large hyperpolarization, an output packet cannot be generated. It can be generated only after the hyperpolarization is gone [Fig. 2(d)], right panel in the top row), when the noise reduction effect is also gone. In contrast, a slow dynamical variable retains the noise reduction effect longer. As shown in Fig. 2(d), the slow variable gets sharpened slowly and remains sharpened when the fast variable has recovered the original state. The enduring narrow width of the histogram of the slow variable sharpens the output packet.

IV. NOISE REDUCTION HAPPENS IN REAL NEURONS

To confirm that the nonlinear noise reduction is biologically plausible, we perform physiological experiments. Whole-cell recordings are performed with slice preparations from the auditory cortex of Wistar rats and a mouse. Detailed setup of the experiment is given in the Appendix B. We can determine the shape of an output packet by performing repeated injections of the input packet along with the background current and measuring firing times [9,13]. The repeated current injections with 400 different realizations of background noise shape the output packet as shown in Fig. 5 with raster diagrams and the firing time histograms, without [Figs. 5(a) and 5(c)] and with [5(b) and 5(d)] the preceding inhibitory input.

Consistently with our theoretical prediction, an output packet is sharpened as long as the membrane potential was near threshold [Figs. 5(a) and 5(b)], where neurons fire spontaneously. The width of the output packet decreases as $\Delta\sigma/\sigma = -23 \pm 19\%$ (from its original width of 3.29 ± 0.84 ms to 2.12 ± 0.69 ms) due to the preceding inhibitory input. In contrast, under the far-threshold condition [Figs. 5(c) and 5(d)], we observe no reliable change: $\Delta\sigma/\sigma = 3 \pm 15\%$ (from 0.89 ± 0.59 ms to 0.86 ± 0.51 ms, $n=5$). The sharpening effects quantified with $\Delta\sigma/\sigma$ under far- and near-threshold conditions are different with the statistical significance (paired t-test, $p < 0.05$).

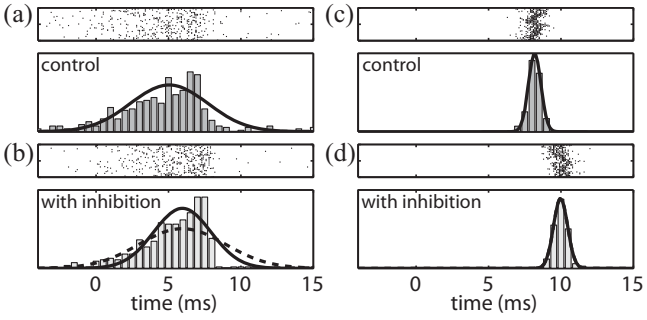

FIG. 5. Experiments using rodent cortical neurons demonstrate the nonlinear noise reduction in a single layer network. (a) and (b) Histograms respectively illustrate output packets obtained in physiological experiments without (a) and with (b) the preceding inhibitory input. The accompanying "raster diagrams" show firing times of neurons for all the trials with dots. The membrane potential of a neuron in slice preparation is set near its firing threshold, which corresponds to point x in Fig. 4(a), by persistent noisy current injection. Such a current injection elicits spontaneous *in vivo*-like firing. The solid curves represent Gaussian fitting of firing histograms. The sharpening of the histogram is clearly seen when the fitting curve in the test case (lower panel) as a dashed curve. (c) and (d) The same as (a) and (b) but the membrane potential is set far from its firing threshold, which corresponds to y in Fig. 4(a). The sharpening of the histogram due to the preceding inhibitory input is not observed. A quantitative comparison of the sharpening effects between near and far-threshold conditions is given in the text.

V. ANALYSIS WITH THE FOKKER-PLANCK EQUATION

In order to understand the nonlinear noise reduction mechanism semianalytically, we analyze the system with FP equations which has proven useful in understanding population behaviors of neurons [16–19]. The FP equations corresponding to a set of equations, Eqs. (1) and (2), are two dimensional so that their numerical integration is computationally demanding. However, the separation of time scale between the fast and slow variables enables us to derive a couple of one-dimensional FP equations of P_v and P_u, which are probability distributions of v and u, as follows:

$$\frac{\partial P_v}{\partial t} = -\frac{\partial}{\partial v}(0.04v^2 + 5v + 140 - \mu_u + I_{syn} + \mu_{bg})P_v + \frac{\sigma_u^2 + \sigma_{bg}^2}{2}\frac{\partial^2 P_v}{\partial v^2}, \tag{3}$$

$$\frac{\partial P_u}{\partial t} = -\frac{\partial}{\partial u}a(b\mu_v - u)P_u + \frac{(ab\sigma_v)^2}{2}\frac{\partial^2 P_u}{\partial u^2}, \tag{4}$$

where μ_{bg} and σ_{bg} represent the mean value and standard deviation of the environmental background current, respectively. To obtain the FP equation with respect to v from Eq. (1), we replace u of Eq. (1) with the mean value, μ_u, for the

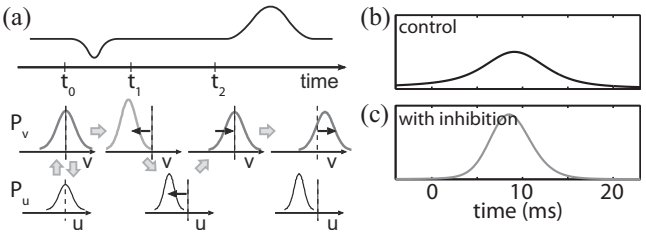

FIG. 6. Pulse packet sharpening demonstrates with the coupled one-dimensional FP equations in a single layer network. (a) Schematic illustration of the one-dimensional FP analysis with adiabatic approximation. The top row represents the input current to the neuronal population: the modulating inhibitory input followed by an input packet. Along the time line, v and u histograms at the times before and after the arrival of the inhibitory input and the times before and after the arrival of the input packet are shown. The gray arrows represent the flows of knowledge: for example, the leftmost up and down arrows indicate that the v histogram is determined from the u histogram and vice versa. The black arrows indicate the directions in which the histograms are moving. (b) and (c) Output packets without (b) and with (c) the preceding inhibition are calculated as above.

drift term of Eq. (3). The corresponding diffusion term consists of the standard deviation of v and the stochastic component of background current, $\sigma_u^2+\sigma_{bg}^2$. Coefficients, μ_u and σ_u, are calculated from the probability distribution $P_u(u)$. Similarly, to obtain the other FP equation, Eq. (4), we replace v in Eq. (2) with the mean value, μ_v and employ the corresponding diffusion term, $(ab\sigma_v)^2$. Note that the dimensional reduction by a separation of time scales is simpler than more accurate version studied previously [28–30].

The boundary condition of Eq. (3) is set to reflect the resetting of v after firing [16]. The boundary condition for Eq. (4) does not precisely account for the tricky resetting, $u \rightarrow u+c$, because this resetting rule only affects the secondary firing which we can neglect when little or no burst firing is expected.

To solve Eqs. (3) and (4), first we determine the equilibrium distribution from our numerical simulations of Eqs. (1) and (2), then we determine $P_v(v)$ and $P_u(u)$ accordingly, which we use as the initial conditions at t_0 to start integrating Eqs. (3) and (4) [see Fig. 6(a)]. The initial values of, μ_u and σ_u, are calculated from those initial distributions. An effect of the inhibitory input can be determined by the integration of Eq. (3) under the assumption that the values of μ_u and σ_u remain unchanged because u is a slow variable. This integration gives us $P_v(v)$ at t_1 [see Fig. 6(a)], which is fitted with the Gaussian function and the values of μ_v and σ_v at that time are determined. With these updated values μ_v and σ_v, we integrate Eq. (4) to see how the delayed noise reduction of the slow variable proceeds. This gives us $P_u(u)$ and therefore μ_u and σ_u at t_2, which is immediately before the arrival of the input. Here, the noise reduction effect that occurred first on v is transferred to u, which is represented as a reduction in σ_u. Finally, we integrate Eq. (3) to calculate how the output packet is sharpened due to the reduction in σ_u. Figures 6(b) and 6(c) show that this approximated FP equations reproduce the sharpening effect.

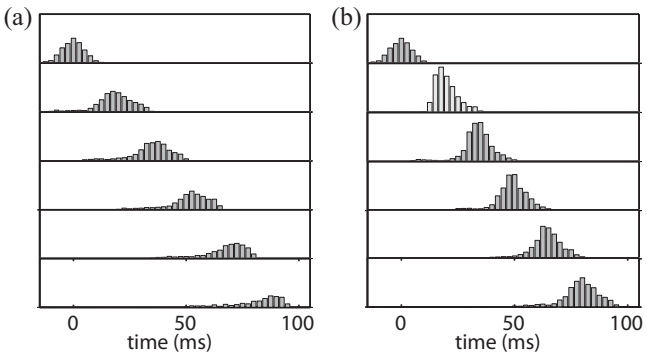

FIG. 7. Impact of inhibitory input expands progressively in later layers. (a) Without the inhibitory input, a weak pulse packet disappears around the sixth layer. (b) With the inhibitory input given only at the second layer, the same initial pulse packet enlarges significantly by the sixth layer.

VI. DISCUSSION

The present study showed that inhibitory input preceding excitatory input enhances the synchrony of population firing. Through the dynamical model analysis, we found that this synchronization is caused by a nonlinear noise reduction mechanism originating in the nonlinearity of the membrane potential dynamics. The nonlinear noise reduction is supposed to be seen in a large class of models with nonlinear subthreshold dynamics and with at least one hidden slow variable. In fact, we demonstrated that the noise reduction happens for the Izhikevich model with different values of parameters and also for the Hodgkin-Huxley model. The nonlinear noise reduction mechanism works optimally when neurons are spontaneously firing. Both the nonlinear membrane dynamics and the spontaneous firing regime are generally found in biologically plausible neurons *in vivo* [31,32]. Although here we considered the noise reduction mechanism in the subthreshold regime, it would be an interesting future direction to study the significance of the nonlinear noise reduction mechanism in the suprathreshold regime.

Figures 7(a) and 7(b) show our simulations demonstrating that the slight difference in the width of a pulse packet caused by inhibitory input only at the initial layer evolves to the noticeable difference in later layers. Thus, nonlinear noise reduction can be powerful enough to control the traffic of the population firing especially in multilayered networks. In recurrent networks, the importance of the nonlinear dynamics has been largely discussed [5,33,34]. The present study complements such studies in that it focuses on the feedforward networks, and studies the significance of the nonlinear membrane potential dynamics there.

A recent monkey experiment showed that the top-down attention signal is targeted mainly to inhibitory neurons instead of more prevalent excitatory neurons [35], suggesting that the attentional signal modulates the network activity via inhibitory input. This peculiar indirect way of modulation looks reasonable in the light of the present finding as well as the previous finding of bidirectional modulation of the firing probability [4]. Such flexible control could work also in other excitable media where nonlinear dynamics is as rich as the neural system.

ACKNOWLEDGMENTS

We acknowledge Yasuhiro Tsubo in RIKEN BSI and Robert B. Levy in NYU for their generous support and advice in physiological experiments. This work was supported by the Special Postdoctoral Research Program of RIKEN.

APPENDIX A: HODGKIN-HUXLEY MODEL

The Hodgkin-Huxley neuron is formulated as follows:

$$C_m \frac{dV}{dt} = -I_{Na} - I_K - I_L + I_{ext}, \tag{A1}$$

where $I_{Na}=\bar{g}_{Na}m_{\inf}^3 h(V-V_{Na})$, $I_K=\bar{g}_K n^4(V-V_K)$, and $I_L=g_L(V-V_L)$ represent the sodium current, potassium current and leak current, respectively. I_{ext} μA/cm^2 is the external current input. Gating variables ($x=h,m,n$) follow first-order dynamics: $dx/dt=(x_{\inf}-x)/\tau_x$. Here, $x_{\inf}$ and τ_x are defined as $x_{\inf}=\alpha_x/(\alpha_x+\beta_x)$ and $\tau_x=\phi/(\alpha_x+\beta_x)$, where $\phi=0.1$ and $x=h,n,m$: $\alpha_h=0.07\exp(-(V+65)/20)$, $\beta_h=1/\{\exp[-0.1(V+35)]+1\}$, $\alpha_m=-0.1(V+40)/\{\exp[-0.1(V+40)]-1\}$, $\beta_m=4\exp(-(V+65)/18)$, $\alpha_n=-0.01(V+55)/\{\exp[-0.1(V+55)]-1\}$, and $\beta_n=0.125\exp[-(V+65)/80]$. The membrane capacitance is set to $C_m=1$ μF/cm^2. The values of the maximum conductance and reversal potential are set as follows: $\bar{g}_{Na}=120$ mS/cm^2, $\bar{g}_K=36$ mS/cm^2, and $g_L=0.3$ mS/cm^2 and $V_{Na}=50$ mV, $V_K=-77$ mV, and $V_L=-54.3$ mV.

APPENDIX B: METHODS OF PHYSIOLOGICAL EXPERIMENTS

Surgical, slicing and recording techniques were done as described previously [13] and followed guidelines established by the NYU Animal Welfare Committee. Slices were made from auditory cortices of young Wistar rats (postnatal day P18 and P19) and a mouse (P21). Whole-cell somatic recordings were made from layer 5 neurons identified under an infrared video microscopy. During recordings, slices (300 μm thick) were perfused at room temperature or at 32 °C with artificial cerebrospinal fluid (125 mM NaCl, 2.5 mM KCl, 25 mM glucose, 25 mM $NaHCO_3$, 1.25 mM NaH_2PO_4, 2 mM $CaCl_2$, and 1 mM $MgCl_2$). Pipettes were filled with 100 mM potassium gluconate, 20mM KCl, 10mM phosphocreatine, 10mM HEPES, 4mM ATP Mg, and 0.3mM GTP at pH 7.3. Filled electrode resistances were in the range of 5–10 MΩ and recordings were performed under current-clamp conditions. Voltage and current signals were filtered and digitized at 10 kHz.

Computer-generated currents (duration 250 ms after removing the initial 100 ms) were delivered to single neuron every 1.6–2.1 s. An input packet was represented by a Gaussian-shaped time course of an input current ($\sigma=5.0$ ms) convolved with alpha function. The intensity of the input packet was adjusted to cause at least 80 % of neural population firing. The inhibitory input preceding an input packet was also described by the Gaussian-shaped current ($\sigma=1.0$ ms) convolved with alpha function and set to cause 5 mV of hyperpolarization. The intensity of Gaussian noise were selected to cause low-frequency spontaneous firing (2–5 Hz) without any input packet and inhibitory input.

[1] W. K. Luk and K. Aihara, Biol. Cybern. **82**, 455 (2000).
[2] R. Dodla and J. Rinzel, Phys. Rev. E **73**, 010903 (2006).
[3] R. Dodla, G. Svirskis, and J. Rinzel, J. Neurophysiol. **95**, 2664 (2006).
[4] T. Shinozaki, H. Câteau, H. Urakubo, and M. Okada, J. Phys. Soc. Jpn. **76**, 044806 (2007).
[5] C. V. Vreeswijk, L. F. Abbott, and G. B. Ermentrout, J. Comput. Neurosci. **1**, 313 (1994).
[6] M. Abeles, *Corticonics: Neural Circuits of the Cerebral Cortex* (Cambridge University Press, Cambridge, 1991).
[7] A. N. Burkitt and G. M. Clark, Neural Comput. **11**, 871 (1999).
[8] M. Herrmann, J. A. Hertz, and A. Prügel-Bennett, Network **6**, 403 (1995).
[9] M. Diesmann, M. O. Gewaltig, and A. Aertsen, Nature (London) **402**, 529 (1999).
[10] M. C. W. van Rossum, G. G. Turrigiano, and S. B. Nelson, J. Neurosci. **22**, 1956 (2002).
[11] N. Masuda and K. Aihara, Phys. Rev. Lett. **88**, 248101 (2002).
[12] Y. Sakai, BioSystems **67**, 221 (2002).
[13] A. D. Reyes, Nat. Neurosci. **6**, 593 (2003).
[14] K. Kitano, H. Câteau, and T. Fukai, NeuroReport **13**, 795 (2002).
[15] K. Kitano, H. Okamoto, and T. Fukai, Biol. Cybern. **88**, 387 (2003).
[16] H. Câteau and T. Fukai, Neural Networks **14**, 675 (2001).
[17] H. Câteau and A. D. Reyes, Phys. Rev. Lett. **96**, 058101 (2006).
[18] K. Hamaguchi, M. Okada, M. Yamana, and K. Aihara, Neural Comput. **17**, 2034 (2005).
[19] K. Ishibashi, K. Hamaguchi, and M. Okada, J. Phys. Soc. Jpn. **75**, 114803 (2006).
[20] J. M. Beggs and D. Plenz, J. Neurosci. **23**, 11167 (2003).
[21] Y. Ikegaya, G. Aaron, R. Cossart, D. Aronov, I. Lampl, D. Ferster, and R. Yuste, Science **304**, 559 (2004).
[22] J.-N. Teramae and T. Fukai, J. Comput. Neurosci. **22**, 301 (2007).
[23] J.-N. Teramae and T. Fukai, Biol. Cybern. **99**, 105 (2008).
[24] B. Doiron, J. Rinzel, and A. Reyes, Phys. Rev. E **74**, 030903 (2006).
[25] E. M. Izhikevich, IEEE Trans. Neural Netw. **14**, 1569 (2003).
[26] C. van Vreeswijk and H. Sompolinsky, Science **274**, 1724 (1996).
[27] C. Holmgren, T. Harkany, B. Svennenfors, and Y. Zilberter, J. Physiol. (London) **551**, 139 (2003).
[28] D. Cai, L. Tao, M. Shelley, and D. W. McLaughlin, Proc. Natl. Acad. Sci. U.S.A. **101**, 7757 (2004).
[29] D. Cai, L. Tao, A. V. Rangan, and D. W. McLaughlin, Commun. Math. Sci. **4**, 97 (2006).
[30] C. Ly and D. Tranchina, Neural Comput. **19**, 2032 (2007).

[31] D. Paré, E. Shink, H. Gaudreau, A. Destexhe, and E. J. Lang, J. Neurophysiol. **79**, 1450 (1998).
[32] T. Hromádka, M. R. Deweese, and A. M. Zador, PLoS Biol. **6**, e16 (2008).
[33] H. Câteau, K. Kitano, and T. Fukai, Phys. Rev. E **77**, 051909 (2008).
[34] T. Aoki and T. Aoyagi, Phys. Rev. Lett. **102**, 034101 (2009).
[35] J. F. Mitchell, K. A. Sundberg, and J. H. Reynolds, Neuron **55**, 131 (2007).